University of Birmingham
Research at Birmingham

Ghost Particle Velocimetry as an alternative to μPIV for micro/milli-fluidic devices

Riccomi, Marco; Alberini, Federico; Brunazzi, Elisabetta ; Vigolo, Daniele

DOI:
10.1016/j.cherd.2018.03.005

License:
Creative Commons: Attribution-NonCommercial-NoDerivs (CC BY-NC-ND)

Document Version
Peer reviewed version

Citation for published version (Harvard):
Riccomi, M, Alberini, F, Brunazzi, E & Vigolo, D 2018, 'Ghost Particle Velocimetry as an alternative to μPIV for micro/milli-fluidic devices', *Chemical Engineering Research and Design*, vol. 133, pp. 183-194. https://doi.org/10.1016/j.cherd.2018.03.005

Link to publication on Research at Birmingham portal

Publisher Rights Statement:
Published in Chemical Engineering Research and Design on 12/03/2018

DOI: 10.1016/j.cherd.2018.03.005

General rights
Unless a licence is specified above, all rights (including copyright and moral rights) in this document are retained by the authors and/or the copyright holders. The express permission of the copyright holder must be obtained for any use of this material other than for purposes permitted by law.

•Users may freely distribute the URL that is used to identify this publication.
•Users may download and/or print one copy of the publication from the University of Birmingham research portal for the purpose of private study or non-commercial research.
•User may use extracts from the document in line with the concept of ‘fair dealing’ under the Copyright, Designs and Patents Act 1988 (?)
•Users may not further distribute the material nor use it for the purposes of commercial gain.

Where a licence is displayed above, please note the terms and conditions of the licence govern your use of this document.

When citing, please reference the published version.

Take down policy
While the University of Birmingham exercises care and attention in making items available there are rare occasions when an item has been uploaded in error or has been deemed to be commercially or otherwise sensitive.

If you believe that this is the case for this document, please contact UBIRA@lists.bham.ac.uk providing details and we will remove access to the work immediately and investigate.

Download date: 25. Apr. 2024

Ghost Particle Velocimetry as an alternative to μPIV for micro/milli-fluidic devices

Marco Riccomi[a], Federico Alberini[b], Elisabetta Brunazzi[a] and Daniele Vigolo[b,*]

[a] *Department of Civil and Industrial Engineering, University of Pisa, I-56126, Pisa, Italy*
[b] *School of Chemical Engineering, University of Birmingham, B15 2TT, UK*
** Corresponding author: d.vigolo@bham.ac.uk*

Abstract

Ghost Particle Velocimetry (GPV) has only been recently introduced and has already been proven useful in small scale phenomena investigations, such as the study of the flow field during single droplets generation in microfluidic devices. In this work, GPV was used to experimentally investigate fluid flow close to a T-shaped branched junction in a millimetre sized device. The experimental setup allowed for the first time, the study of complex fluid dynamic structures such as vortices and recirculation zones. Several experiments were performed to exploit the capability of GPV in carrying out flow field measurements, at different Reynolds numbers within the laminar flow regime and for two channel sizes. The results were validated by verifying the steady state and stability conditions and by comparing them with results obtained using the well-established micron-scale Particle Image Velocimetry (μPIV). Differences between these two velocimetry techniques were analysed in terms of qualitative and quantitative parameters, to attain a performance comparison and understand the strengths and weaknesses of each respective method.

Keywords: Ghost Particle Velocimetry; μPIV; Experimental fluid-dynamic; Particle velocimetry; T-junction.

---

1. Introduction

Micro/milli-fluidic devices have turned into increasingly popular tool in many chemical, medical, pharmaceutical, biological, and many other applications, both in academic and industrial settings (Hessel et al., 2005; Lee et al., 2016; Orsi et al., 2013a; Roberge et al., 2005; Rossetti and Compagnoni, 2016). Diagnostic methods for elucidating flow regimes and structures within these systems have similarly become central to their successful design and optimisation. Numerical simulations are a powerful tool for flow investigations, particularly in small scale domain, where three-dimensional (3D) flow reconstructions are usually accomplished satisfactorily (Vigolo et al., 2014). However, experimental tests are required to assess and validate the numerical predictions (Mariotti et al., 2018), especially when chemical reactions (Bothe et al., 2011), complex rheology (Galletti et al., 2015; Poole et al., 2013) and unsteady flow regimes (Fani et al., 2014; Galletti et al., 2017) are present in the system. The fluid flow velocity can be experimentally measured in different ways exploiting a number of particle velocimetry techniques. Within this category, the µPIV is commonly used due its reliability and availability on the market of several commercial turnkey systems and dedicated software (Adrian and Westerweel, 2007). This technique allows to evaluate the planar components of the velocity on sections of the device, by "tracking" small fluorescent tracers that follow the fluid motion (Jahanmiri, 2011). However, µPIV requires a rather expensive instrumentation, which includes a double pulsed laser, synchronised with a high-resolution camera connected to the specimen via a complex optical setup. A new velocimetry technique known as the Ghost Particle Velocimetry (GPV) has recently been introduced (Buzzaccaro et al., 2013), which, just like µPIV, is based on imaging and cross-correlating small tracers' displacements (Brossard et al., 2009). In contrast, the distinctive feature of this technique is the use of the speckle pattern produced by nanoparticles with high refractive indices instead of signals emitted by fluorescent micro- or nano-seeding particles. The speckle pattern is the result of the constructive and destructive interference of the light scattered by the nano-diffusers which identifies the tracers and dynamically follows their motion. Thus, the speckle pattern can be utilised to perform the displacement analysis by means of an algorithm similar to that used for PIV. It is useful to emphasise that the in-plane speckle's characteristic size, δ_x, is lightly affected by the optical setup in far-field analysis (i.e. it is essentially not influenced by the objective magnification) while in near field optics the size of a speckle is the same as the size of a tracer (Buzzaccaro et al., 2013). This characteristic size is defined as $\delta_x \approx \lambda / NA_C$, where λ is the wavelength of the light used and NA_c is the numerical aperture of the condenser. In the conducted experiments, the value of NA_C was adjusted between 0.15 and 0.20 which translates to a characteristic far-field speckle diameter of about 3 µm (Asakura and Takai, 1981; Cederquist et al., 1988; Dainty, 1975). This simplifies the velocimetry investigations in small scale devices because the optical magnification is higher and the tracers are small enough to not disturb the fluid flow field, thus the speckle pattern is easier to detect. The speckle pattern formation can be observed with coherent light illumination, otherwise, no speckle pattern will be identified as incoherent light scattered by nanoparticles sums up randomly, preventing the formation of detectable speckles. GPV exploits the standard bright field illumination of a microscope, thus an inherently incoherent light, to generate a speckle pattern by manipulating its properties and converting it into a partially coherent illumination source. This is done by reducing the numerical aperture of the condenser lens by manually closing the condenser aperture diaphragm of the optical microscope. The peculiar spatial coherence properties of the illumination source, besides providing a good contrast of the speckle pattern on the transversal (in-plane) field of view, allows for a finite longitudinal resolution along the optical axis (Buzzaccaro et al., 2013). This means that the speckle pattern observed originates from a well-defined volume within the sample and hence, a 3D flow visualisation and quantification can be attained. The longitudinal resolution is determined by $\delta_z \approx \lambda/(NA_C)^2$, which translates to a resolution of few tens of microns (Buzzaccaro et al., 2013). Another advantage of this technique is that it does not require the use of a laser, making the experimental arrangement more compact, simpler and more affordable in comparison to the PIV technique. Finally, GPV has demonstrated excellent results in recent fluid-dynamic investigations within microfluidic devices, where single droplets formation in flow focusing devices were extensively analysed (Kovalchuk et al., 2018; Martino et al., 2016; Pirbodaghi et al., 2015). The interesting features of these studies have all been combined in this work by using GPV for the first time to investigate the vortical flow structures occurring at relatively high Reynolds numbers in a T-branched junction responsible for particle trapping (Vigolo et al., 2014), to assess its performance and compare it with the well-established µPIV.

2. Materials and methods

2.1 Device geometry and preparation

In this work, two milli-fluidic devices with identical geometries but different characteristic lengths (channel lateral size, L) were investigated. The T-branched junction systems were composed of a straight inlet with a square cross section that splits into a bifurcation. The flow regime considered is laminar and the flow is completely developed before reaching the junction. The size of the two square section branches are the same as the size of the inlet, which joins back together to produce a single outlet. In this way, the pressure on the two outlet branches of the flow splitter are perfectly equalised, and the geometry is entirely symmetric (Ault et al., 2016).

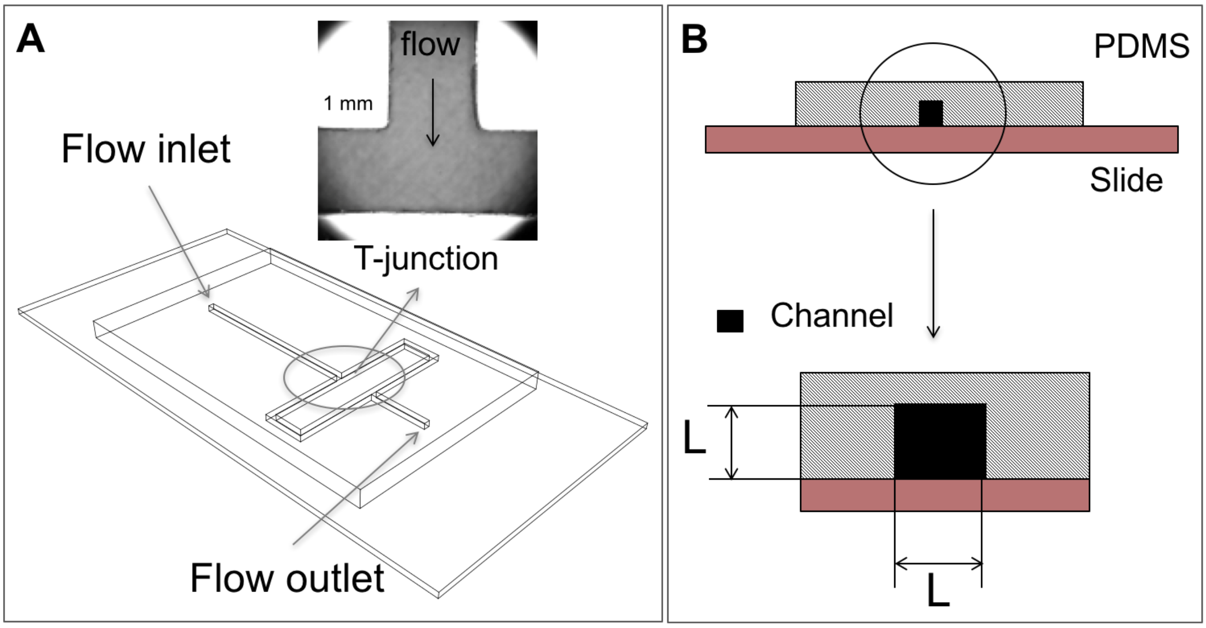

Figure 1: Schematic of the device and a 4x microscope image of the branched junction (A), lateral view of the square cross-section of the device inlet (B).

The fluid enters at the beginning of the straight channel and travels throughout the T-shaped junction before leaving the system. The fluid dynamic investigation is focused on the bifurcation, as shown in Figure 1, where the device's lateral view is also displayed. The channels, with a lateral size L of *1* and *2 mm*, were fabricated by designing a specific manufacturing procedure detailed as follows:

(i) The Formlabs® Form 2 desktop 3D printer was used to create a high-resolution (superficial finishing of 25 µm) acrylic base plastic mould of the channel;

(ii) A standard 1:10 curing agent to base ratio of Polydimethylsiloxane (PDMS, Sylgard® 184, Dow Corning) is poured in a petri dish to completely cover the mould, which was previously attached to the plastic container with a strong glue;

(iii) The petri dish was maintained under vacuum condition (150 mbar) for 30 min to remove possible entrapped air bubbles, and cured in an oven at 70 °C for about 2 hours. The PDMS device was then carefully removed;

(iv) A corona discharge device (Relyon, PZ2) was used to activate the PDMS surface and weld the silicon to a glass microscope slide.

2.2 Experimental set-up

GPV and µPIV experimental arrangements, used in the present study, are shown in Figure 2. The main differences are the illumination sources and the camera technology. Other distinctive characteristics can be found in the required microscope components and tracer size.

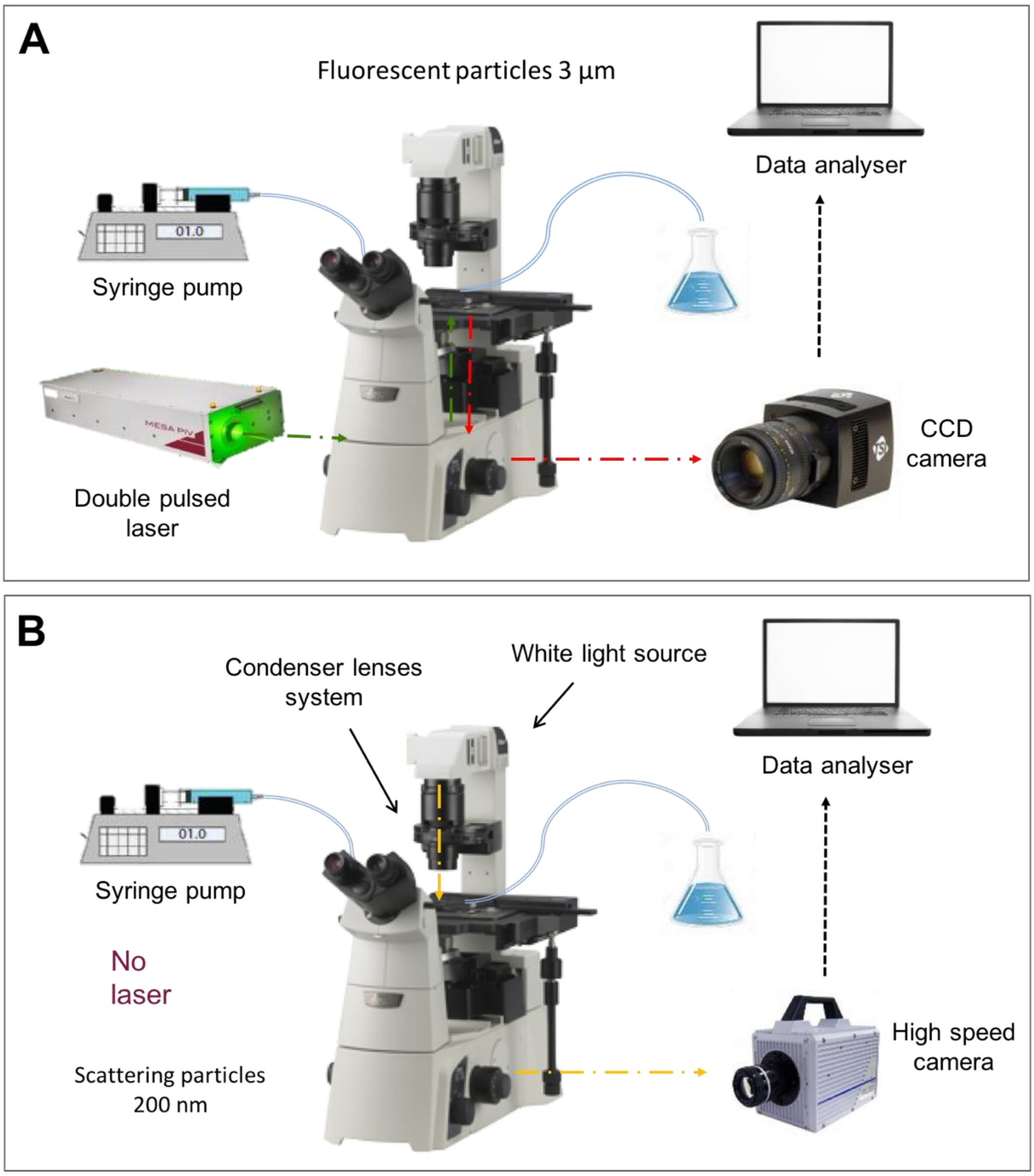

Figure 2: The schematic rig of the μ PIV experimental setup (A), and the GPV's setup (B).

The µPIV setup is a standard turnkey system directly supplied by TSI® Inc. It is composed by a high power (400 mJ) double pulsed Nd-YAD laser (532 nm and 10 ns of pulse duration), electronically synchronised with a high-resolution CCD (Charge Coupled Device) camera (Powerview plus 4MP) and connected with an optical fibre to the microscope. The inverted microscope (Nikon Eclipse TE2000) is equipped with dichroic mirror to visualise only the fluorescence contribution of the light emitted by the tracers. The GPV setup, instead, is based on a Nikon Ti-U Eclipse inverted microscope, the illumination source is a white LED light and it is equipped with a condenser lens with adjustable numerical aperture. The Photron SA5 high speed camera (1MP at 7000 fps), directly mounted onto the microscope, was used to record the speckle pattern. In both the arrangements the seeded fluid flows inside the system pushed by the Harvard PHD 2000 syringe pump, which allowed the setting of constant volumetric inlet flow rates. A 1.6 mm ID PVC tubing connected the syringe to the devices and collected the exiting fluid to a receiver beaker.

2.3 Flow conditions

The working fluid for both velocimetry techniques was deionised water at controlled room temperature seeded with a small concentration of tracers. For the µPIV the 3 µm fluorescent tracers (Duke scientific polymer microspheres red fluorescing) were added to the fluid until the optimal seeding concentration was reached for the best possible velocity vectors reconstruction. For GPV, 200 nm polystyrene particles (Sigma-Aldrich) with a concentration of 0.1% w/w (see Section 3.1) was used. In both cases, the particle suspension is diluted and the fluid dynamic interactions between the tracers were negligible. Moreover, the seeding particles are small enough to faithfully follow the fluid motion and not disturb the flow field, for instance, the corresponding Stokes number is a numbers of magnitude lower than one (St ≈ 10^{-3} - 10^{-4}):

$$St = \frac{\rho_p \, d_p}{18 \, \mu} \qquad (1)$$

where ρ_p is the particle density, d_p the particle diameter and µ the fluid dynamic viscosity (water in this work). The Reynolds number of the inlet flow rate is used to characterise the fluid-dynamic conditions of the system and is defined as:

$$Re = \frac{\rho \, U \, L}{\mu} \qquad (2)$$

where U represents the superficial velocity of the flow at the inlet straight channel of lateral size L and ρ is the fluid density.

For both the devices (L = 1 and 2 mm), four inlet flowrates, corresponding to Re= 50, 150, 250 and 350, were used to pinpoint the significant fluid-dynamic features that evolve close to the branched junction and to compare the two experimental techniques. The volumetric flowrates adopted for the experiments are summarised in the next Table 1.

Table 1: Volumetric flowrates, superficial velocity and corresponding Reynolds numbers used for the investigations.

Re	**L = 1 mm**		**L = 2 mm**	
	Flow rate (ml/min)	**U (mm/s)**	**Flow rate (ml/min)**	**U (mm/s)**
50	3.0	50	6.1	25
150	9.1	150	18.2	75
250	15.1	250	30.3	125
350	21.2	350	42.4	175

2.4 Image processing procedures

The frame sequence of the injected suspension, for both the velocimetry techniques, has to undergo an image processing procedure to extrapolate the flow velocity field. As can be seen in Figure 3A, the seeding and the speckle pattern are not visible in the GPV's recording. The tracers are not captured by the camera sensor, because their characteristic size is below the white light diffraction limit (~ 300 nm), whereas the contribution of the light scattered by the nanoparticles is basically masked by the stronger transmitted beam.

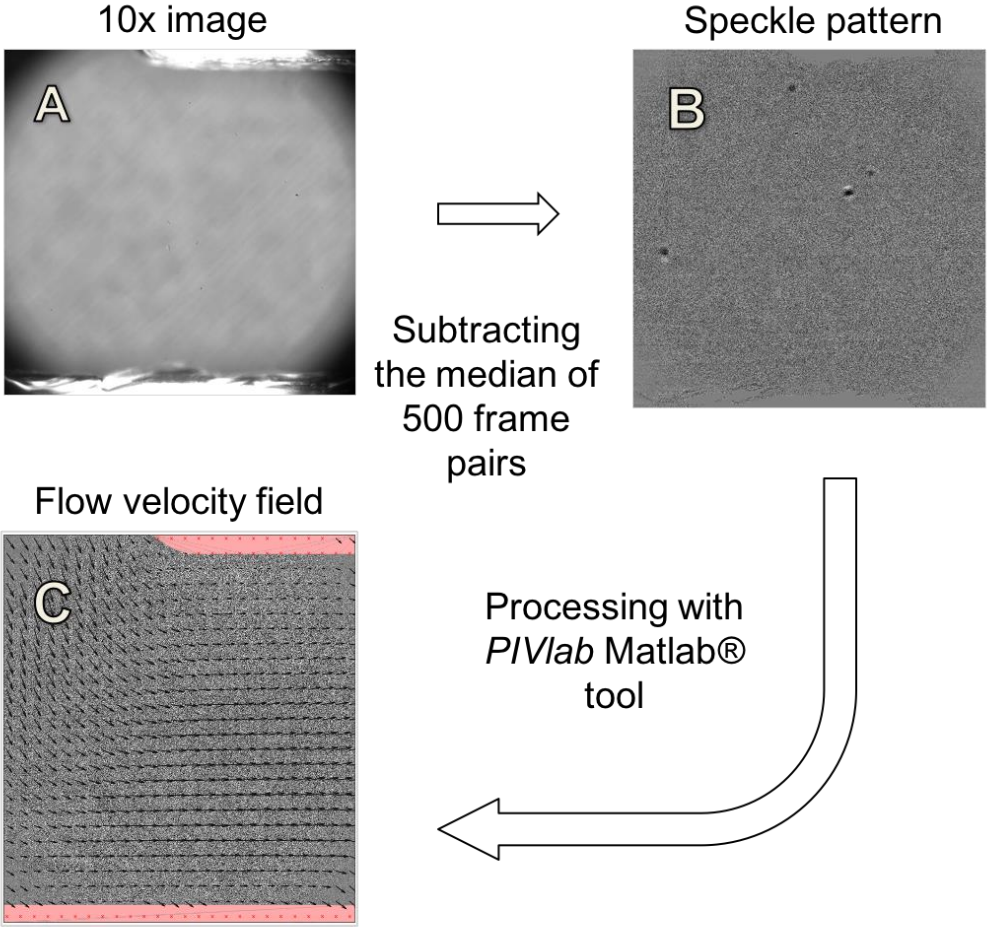

Figure 3: Tracers and speckle pattern are invisible to the camera's sensor (A), but the scattering speckle pattern becomes apparent after the static background elimination by subtracting the median of several images (> 100 frames) (B). Now the cross correlation of the speckle pattern can be used to reconstruct the flow velocity field (C).

A well-defined speckle pattern becomes apparent by removing the background static contribution from the images, as shown in Figure 3B. This was done by subtracting the median of a large number of frames (500, in this work) from each image of the sequence (Pirbodaghi et al., 2015). In this way, the time-independent contribution is removed and the speckle pattern clearly appears in every frame of the video. In this condition, each two consecutive frames of the image sequence can be cross-correlated to reconstruct the 2D flow velocity field (see Figure 3C). In the present work, the latter has been performed using PIVlab, an open source Matlab® routine (Thielicke and Stamhuis, 2014). The high speed camera records a "continuous" sequence of frames, which implies that, unlike in the µPIV case, the images are not separated by a specific repetition rate (Adrian and Westerweel, 2007), but the time interval is directly forced by the camera's frame rate (FR). More precisely, every frame is captured in single camera sensor exposure, therefore a sequence of images spaced out (in time) by the inverse of the frame rate is created. By coupling the images in proper sequencing style (usually 1-2, 2-3, 3-4, etc.), the series of the frame pairs required for the velocimetry analysis is made up. Before each run, the injected solution was sifted several times with a 10 μm syringe filter, to minimise the presence of impurities. Nonetheless, these are sometimes present in the flow (see Figure 3B) and might generate erroneous vectors in the cross-correlation analyses. However, the image processing procedure allows to easily discard these vectors, as the velocity vectors calculated in the cells occupied by the impurities tend to be different (in direction and magnitude) from the ones generated by the speckle pattern. On the contrary, the images acquired using µPIV require minimal processing. The fluorescent tracers used have a characteristic size significantly higher than the diffraction limit, thus they are imaged as bright dots in the raw frame pairs. Insight 4G software, directly supplied by TSI® Inc., was used to collect the video recorded to perform the displacement evaluation. The cross-correlation analysis within the PIVlab Matlab® routine and Insight 4G software has been performed by using the same image processing settings. A double pass correlation was selected for both techniques; the first pass uses a square cell of 64 x 64 pixels for the μPIV and 32 x 32 pixels for the GPV analyses (see Section 0). In the second pass, the interrogation region was reduced to 32 x 32 pixels and 16 x 16 pixels for the μPIV and GPV respectively. For both the particle image techniques, the FFT window deformation cross correlation algorithm with a linear window deformation and a correlation step of half the cell's size were implemented. Both experimental techniques produced a text based file (.csv format for PIVlab, and .vec for Insight 4G) containing the planar velocity components at each point of the plane investigated. These files were processed with custom made Matlab® scripts to automatically display the results in a fully editable contour plot.

2.5 Interrogation region and timing setup

The interrogation region size (L_{IR}) and the acquisition time between successive frames (Δt) are two crucial parameters for the optimal flow field reconstructions. The interrogation region (IR) represents the area where the software calculates a single velocity vector, whereas the second parameter indicates the time intervals between the frame pairs. Both of these parameters are strictly linked to the particle displacements and thus, their respective values were chosen properly to assure consistent analysis. The L_{IR} was chosen in order to include enough tracers (being these the fluorescent particles or the speckles) within the IR to obtain statistically relevant displacement information. The µPIV's IR size was set to 64 x 64 pixels, to ensure a good density of vector in the flow field. Considering the different resolution of the camera used by the GPV (see Section 0), the dimension of 32 x 32 pixels was chosen for the investigations. Through this, the vector density of the images collected using the two techniques is perfectly comparable. The selection of Δt was calculated based on the fluid flow speed, i.e. to the characteristic time of particle's motion (τ_f). A heuristic guideline to calculate Δt is given in the TSI® Inc. official technical report, which suggests getting a quarter of the time required by the particles to cross the IR's main dimension. This concept is converted into a mathematical expression as:

$$\Delta t = \frac{1}{4}\tau_f = \frac{1}{4}\frac{L_{IR}}{U} \qquad (3)$$

The value calculated is considered a reasonable approximation, assuming that an averaged velocity was used. Indeed, the values evaluated with the heuristic method (using Eq. 3) was taken as first attempt, which has been improved with further tests (also because a double pass correlation has been used in the cross-correlation algorithm, see Section 2.4). While for µPIV the time interval was set in the timing setup window of the Insight 4G software, for the GPV this is done by selecting the frame rate of the high speed camera (see Sec. 0). The corresponding time interval is the inverse of the frame rate. Table 2 shows the time intervals used in the experiments for different flow conditions as well as the camera frame rate for the GPV.

Table 2: Time interval between respective images in an image pair for different flow conditions.

Re	$\Delta t_{\mu PIV}$ (μs)		Δt_{GPV} (μs)		FR_{GPV} (fps)	
	1 mm	2 mm	1 mm	2 mm	1 mm	2 mm
50	250	500	200	333	5 000	3 000
150	83	166	67	167	15 000	6 000
250	50	100	50	100	20 000	10 000
350	35	70	33	67	30 000	15 000
400	31	62	25	50	40 000	20 000

3. Results

T-junctions (both splitters and mixers) are among the most commonly used micro-devices due to their simple geometry. Often these geometries can be found in more complex micro-reactor networks. In addition, T-junctions show unique flow topology and complex flow structures in the laminar regime, both in T-mixers and in T-splitters. In this regard, T-mixer have been largely investigated in the literature, both experimentally and numerically (Bothe et al., 2006; Engler et al., 2004; Fani et al., 2013; Galletti et al., 2017, 2015, 2012; Hoffmann et al., 2006; Kockmann et al., 2006; Lindken et al., 2006; Orsi et al., 2013b; Soleymani et al., 2008; Thomas and Ameel, 2010). These works mainly focus on the flow regimes and mixing performances by investigating the flow field developing when the two fluids meet at the junction for different configurations and at varying Re numbers. Moreover, the fluid-dynamic features regarding the configuration used in this work (see Sec. 0) which presents a single inlet splitting into two outlets, have also been explored in other works. For instance, in a research conducted at the University of Princeton, USA, Vigolo et al. (2013) used the T-shaped bifurcation to study the particle-wall impact in an abrupt direction change. This investigation highlighted the development of unexpected complex flow structures in the system, such as vortices and recirculation regions that were clarified in their subsequent studies. In Vigolo et al. (2014), the fluid flow was characterised by 3D numerical simulations, video flow recording and two-phase forces balance while in works by Ault et al. (2016) and Chen et al. (2015), 3D Direct Numerical Simulations (DNS) and flow visualisation experiments were carried out to investigate the flow features in different junction geometries and to demonstrate a correlation between these and the classical vortex breakdown structures present in a rotating container or the flow over a delta wing (Benjamin and Benjamin, 1962; Hall, 1972). The selected operating conditions described in Ault et al. (2016) and Vigolo et al. (2014) were adapted in this paper, to compare the flow velocity fields obtained from the two optical techniques. All the experimental results shown in this work refer to the red rectangle region depicted in Figure 4.

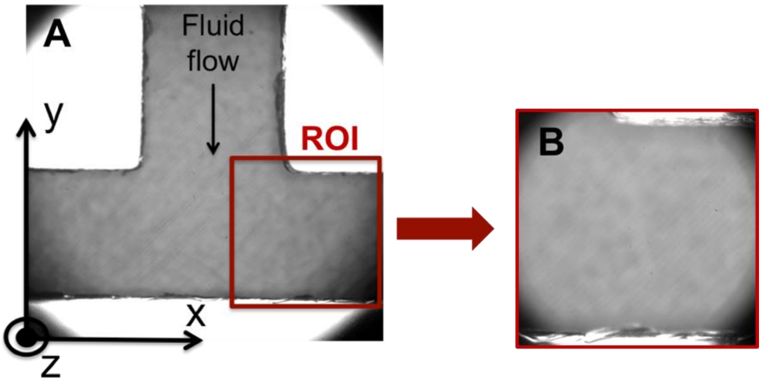

Figure 4: A, the 4x magnification of the T-junction and, B, the Region of Interest (ROI, the red rectangle), where all the tests performed are focused on.

In order to observe the most interesting flow structure, the normalised mean horizontal component (i.e., the local horizontal component of the velocity, normalised by the inlet superficial fluid velocity, U) of the velocity has been drawn in the contour plots reported in the following. The word "mean" is related to the fact that the displacement analysis is realised over an adequate number of different frame pairs, and the final result is the arithmetic average of local velocity calculated in each frame pair. This is the classical procedure performed in steady state problems, where the velocity flow field is time independent (Brossard et al., 2009). The mathematical process is:

$$\bar{u}_n(x,y) = \frac{1}{U}\sum_{i=1}^{N}\frac{1}{N}u_i(x,y) \quad (4)$$

Where N is the number of frame pairs utilised for the test, u_i is the local horizontal component of the velocity evaluated at the i-th frame pairs, while $\bar{u}_n$ is the normalised one. In Figure 5, the results obtained with the two velocimetry techniques at four Reynolds numbers are compared, showing a good qualitative and quantitative agreement. The investigations reported here were performed with the 2 mm device and are focused on the plane at 350 μm of depth from the channel's bottom, where, at high Reynolds numbers, the recirculation loops develop (Vigolo et al., 2014). The velocity profiles shown in Figure 5 are obtained from the contour plots for different Reynolds number and show the horizontal component of the velocity, u_N, along the y direction at a fixed x position ($x = \frac{x_{MAX}}{2}$). It is possible to appreciate how the agreement between GPV and µPIV is good especially at low Reynolds numbers whereas at higher Re the two profiles, although qualitatively similar, start to differ appreciably. All the contour plots in Figure 5 refer to the ROI shown in Figure 4. It is considered worthwhile to underline as the same IR density has been used in all the contour plots (see Sec. 0), therefore the number of calculation cells per unit area were kept constant, i.e. there are no differences in terms of number of vectors per area between the pictures. Furthermore, all the contour plots have the same colour map, defined by the colour bar visualised within Figure 5.

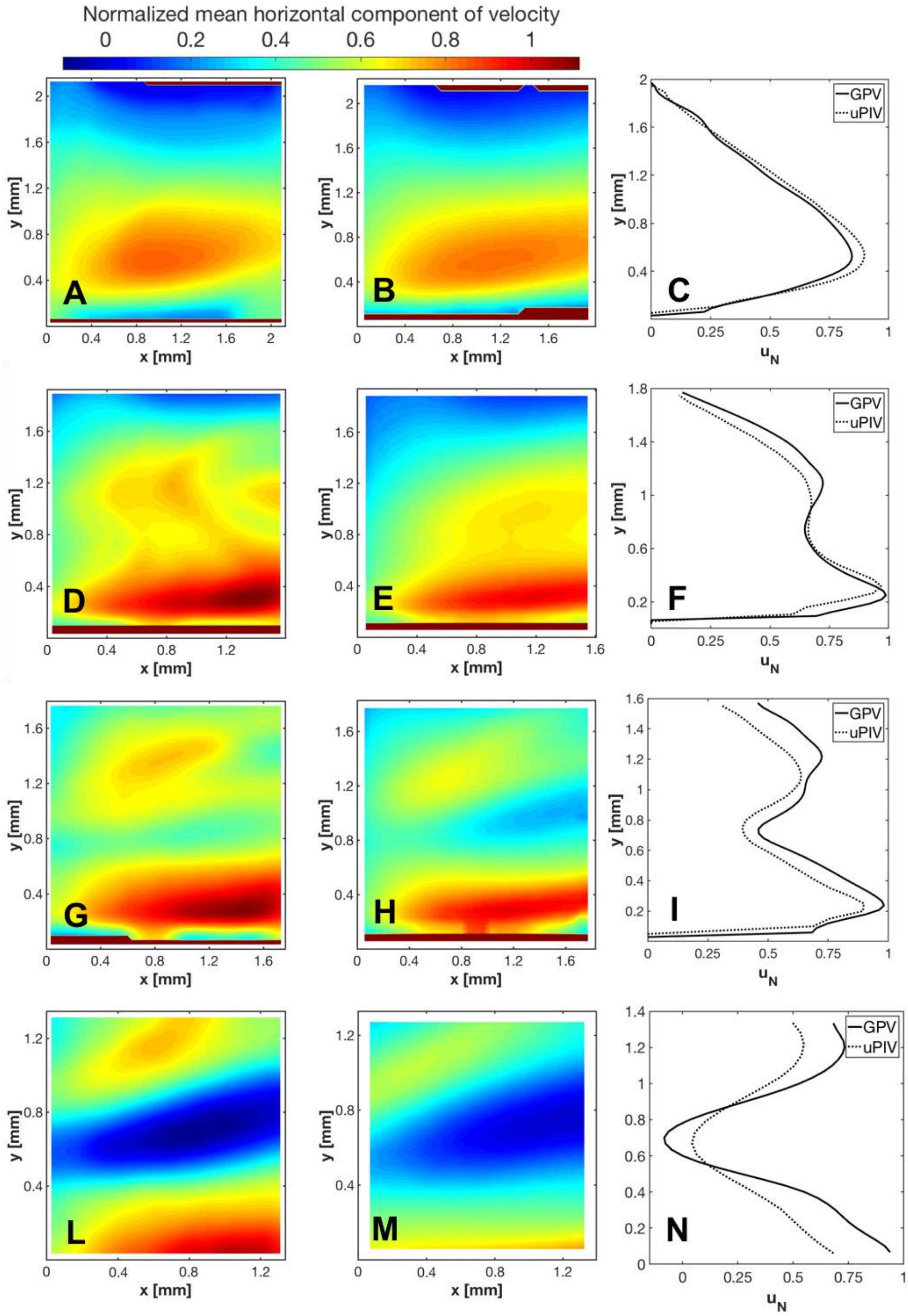

Figure 5: First two columns from the left: flow velocity fields obtained with GPV (A, D, G, L) and µPIV (B, E, H, M) for Reynolds numbers 50 (A, B), 150 (D, E), 250 (G, H) and 350 (L, M) at a height z = 350 µm measured from the channel's bottom. Third column from the left: normalised mean horizontal velocity profiles, u_N, along the y direction obtained from the contour plots at $x = \frac{x_{MAX}}{2}$, for Reynolds numbers 50 (C), 150 (F), 250 (I) and 350 (N).

Figure 5A and Figure 5B show the results obtained, at Re=50, with the GPV and µPIV, respectively. In both the images it can be seen an elliptical region towards the lower edge of the channel (the red one) with higher velocity; outside this area the horizontal component of the velocity starts to decrease until values tend to zero (near the walls). The fluid flow is disturbed by the abrupt direction chance but any significant flow features can be recognised. At Re=150 (Figure 5D and Figure 5E) the fastest dark red coloured region is thinner and shifted towards the bottom (along the y axis) of the channel. The faster fluid flow is closer to the lower edge of the channel and this is due to the presence of a vortex that develops, starting from Re=100, in the region immediately above (Vigolo et al., 2014, 2013). The vortex structure becomes clearer at Re=250 (Figure 5G and Figure 5H) where a central slower region (the blue one) can be observed in both the contour plots. As can be noticed, the slower central region in the µPIV image is wider, this is probably due to the fact that the two images are not exactly centred in the same plane as they refer to two different experimental setups. Nonetheless, the qualitative agreement remains remarkable. In this fluid-dynamic state, the flow profile becomes strongly dependent on the longitudinal coordinate (z axis, depth of the channel), therefore also a small mismatch in the plane's selection may generate a significant variation of the result. The fastest zone is now pushed even further towards the lower wall. In the last two contour plots (Figure 5L and Figure 5M), the result obtained at Re=350 is shown. For a T-junction at Reynolds number 350 and above (different junctions have different critical Reynolds numbers (Ault et al., 2016)) a region where the horizontal component of the velocity assumes a direction opposite to the main fluid flow developed into the channel, this means that part of the liquid is recirculated towards the junction centre. All the results perfectly agree, in both the velocimetry techniques, with previous works (Vigolo et al., 2014) especially regarding the flow complex structure nature and locations over the different fluid-dynamic states. Moreover, the GPV shows outcomes definitely similar to the well-established µPIV, confirming the validity of GPV as a promising alternative to the more expensive µPIV. It is nonetheless worth remember that GPV and µPIV both show the flow pattern obtained from the average over a finite volume which thickness is different from the two techniques. In particular, in the GPV this is only related to the numerical aperture of the condenser (see the Introduction section) while for µGPV this depends on the magnification used. This translates in a slightly different absolute value of the velocity measured by the two techniques, and this partly justify the differences in the contour plots of GPV and µPIV.

3.1 Seeding optimisation

In order to assess the optimal seeding concentration for our GPV's experiments, several tests with different seeding concentration, c, have been carried out, in particular we explored a range from about 0.01% to 0.3%. The normalized mean horizontal component of velocity after five hundred frame pairs were evaluated at three points (see Figure 6) in the investigated plane (z = 350 μm), by using the $2\,mm$ device at Re = 250 seeded with different particles concentrations. The results are summarised in Figure 6, where three regions, divided by two black dotted lines, can be identified:

I. $c < 0.05\%$: the tracers' concentration is too low inside the interrogation region, and so the algorithm does not have enough speckles to track the fluid flow

II. $0.05\% < c < 0.15\%$: the differences between the normalised horizontal component of the velocity values are rather small, so the velocity calculated is independent on the particles concentration. The result can be considered stable and consistent;

III. $c > 0.15\%$: the high concentration of tracers inside the interrogation region does not allow a proper cross-correlation. This is typical of any particle image velocimetry technique in general and GPV seems to be affected as well.

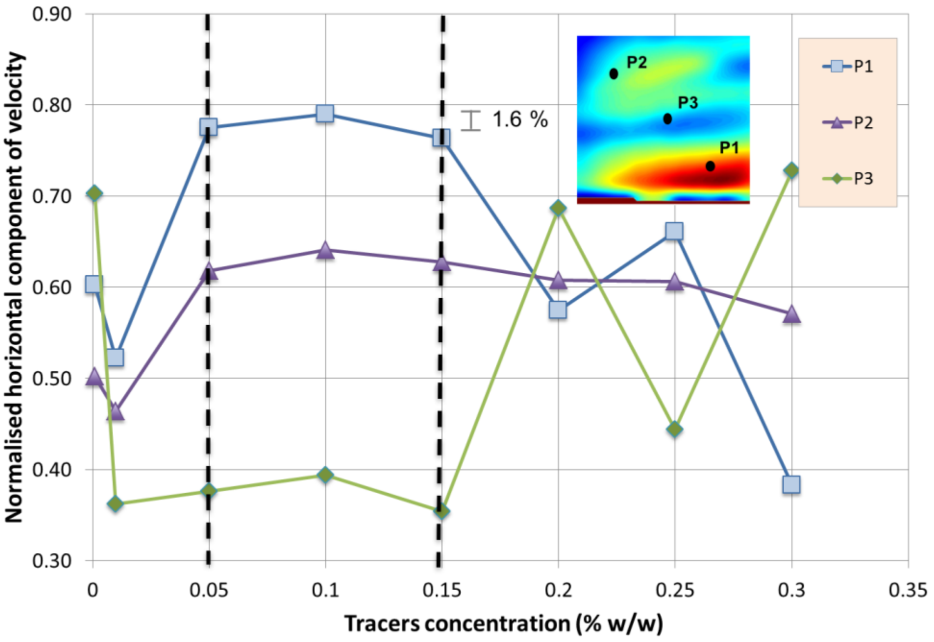

Figure 6: Seeding optimisation for the GPV’s experiments.

The investigations have highlighted the existence of a concentration range, outside of which the speckle pattern’s quality is not sufficient. The reason has to be found in the geometrical characteristics of the device. In particular, in the present work the devices have a typical dimension in excess of a millimetre, larger than any previous work on GPV. As a result, in our experiments, along the optical path the number of light scattering events is higher, thus the speckle pattern signal presents a higher degree of noise. This phenomenon tends to smooth the raw images, the contrast between the speckles and the background becomes lower, so they are barely recognisable and the results decay. This is why in our experiments, a lower particle's concentration has permitted to obtain better flow velocity fields (by reducing the multiple scattering). A more accurate investigation on the described phenomenon could bring to define the mathematical correlation between the tracer's concentration and the size of the channel but it has been considered outside the goals of this work.

3.2 Steady state and stability validation

In all the tests, the fluid-dynamic regime is laminar and steady state, hence the local velocity has to be time independent. This condition must be satisfied by both the optical techniques to assure the consistency of the velocimetry analysis. To check the diagnostic method's reliability, the normalised mean horizontal component of the velocity was monitored in five points chosen over the studied plane (their locations can be seen in Figure 7 and they are selected to represent different scenarios in the flow field). The reference for the validation is a Cartesian diagram, where the $\bar{u}_n(x, y)$ velocity is plotted as a function of the number of frame pairs utilised for the reconstruction. The investigation carried out for the 2 mm device at Re=150 in the GPV's experiment is reported in Figure 7.

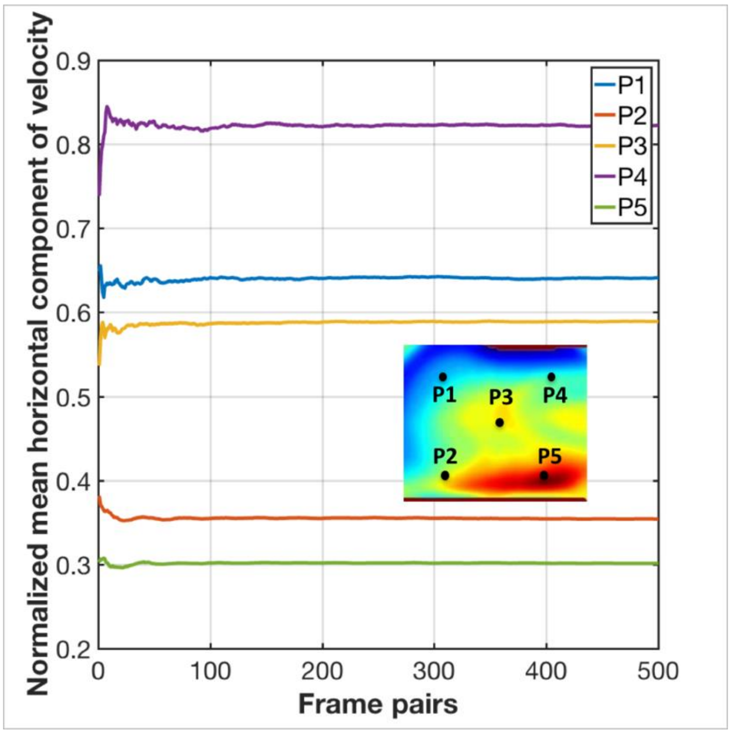

Figure 7: Steady state and stability validation for the 2 mm channel at Re=150. The normalised mean horizontal component of velocity is shown as a function of the number of frame pairs. The window reports the location of the five points monitored on the plane analysed.

Each line of the plot represents the $\bar{u}_n(x, y)$ evolution on varying the number of frame pairs employed for the velocity calculation, thus every point of the line represents the results of the arithmetic average between all the previous frame pairs (see Sec. 0). The local normalised velocity fluctuates at the beginning, but it converges to a fixed and constant value after a certain number of image pairs. The latter value represents the minimum amount of frame pairs required for a consistent velocity evaluation. When the number of frame pairs used is higher than the minimum, the analysis can be considered stable, congruent and time independent. This kind of study has been performed in every experiment for both the optical techniques, as the one pointed out in Figure 8, concerning the GPV's investigation on the 1mm device.

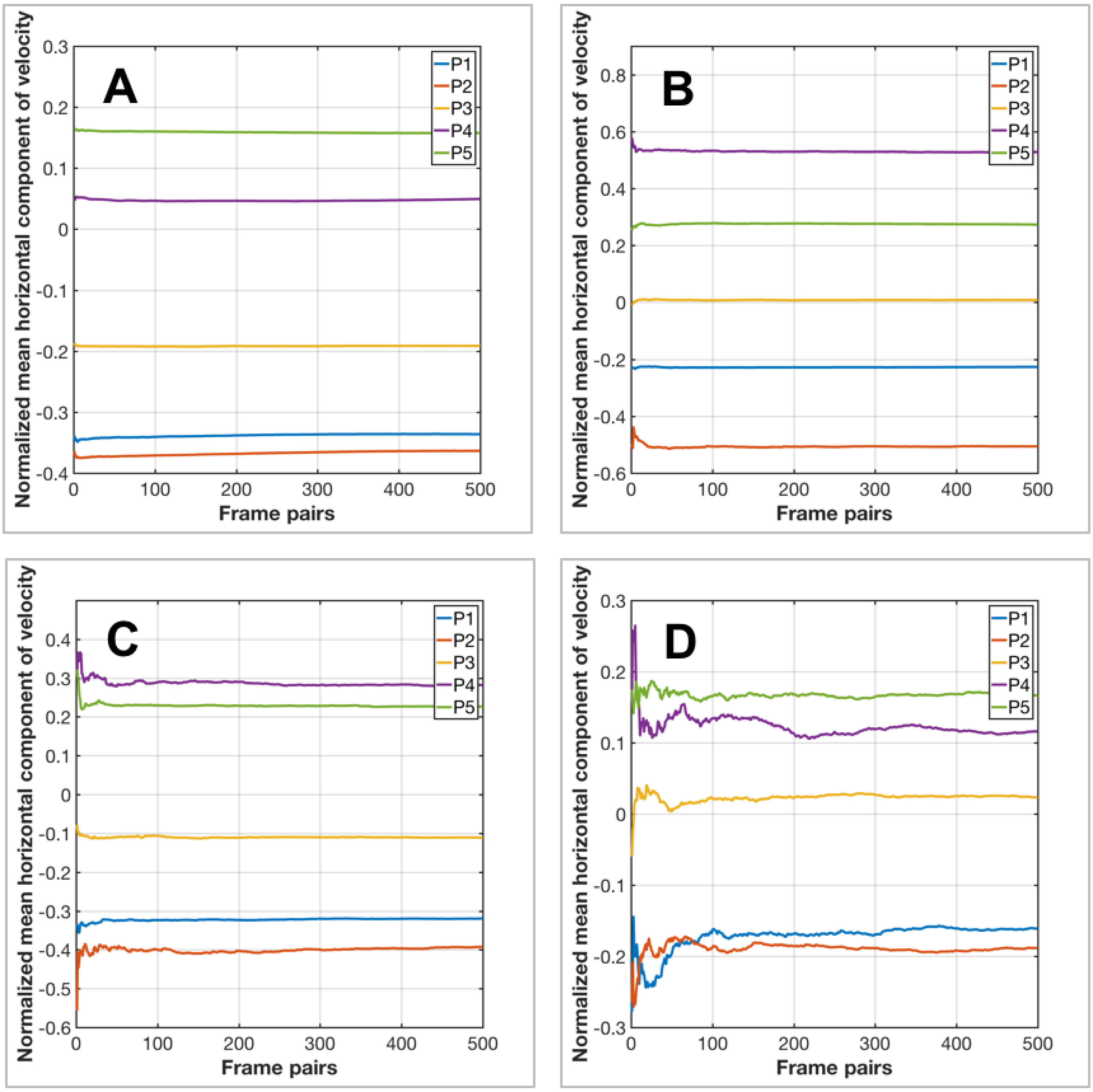

Figure 8: Steady state and stability validation for the 1mm device at different Reynolds numbers: 50 (A), 150 (B), 250 (C) and 350 (D). Each line refers to a specific location within the channel as described in Figure 7.

As it can be noticed, all the analyses are stable and time independent, but the number of frame required to achieve the convergence rapidly increases when the Reynolds number becomes higher. By increasing the fluid flow speed, the GPV requires a higher camera's frame rate for the reconstructions (see Sec. 0) and at the same time the electronic noise surges; therefore, the frame sequence recorded has a lower quality. The speckle pattern contrast tends to be reduced, hence its identification is harder and the technique's performance deteriorates, as better illustrated in Sec. 3.3. Ultimately, if the normalised mean horizontal component of the velocity has not achieved a stable trend using 500 frame pairs, the analysis has not been considered valid and the results have been discarded. This is the case of the GPV reconstruction at Re=400, which has not been shown in the flow velocity fields comparison section. It is important to mention that this is simply a limitation of the fast camera setup available. A higher specs camera, presenting a higher signal to noise ratio would have enabled us to measure higher flow rates exploiting the GPV technique.

3.3 Strength and weaknesses of the diagnostic techniques

Through the comparison with the µPIV, as well as the validation of the time independence and convergence of the outcomes, the GPV has demonstrated to have the potential to achieve remarkable results. What follows is the quantification of the performance of both diagnostic techniques. The aim is to realise a comparison between the velocimetry techniques, defining quantitative parameters that allow emphasising their major weaknesses and strengths at varying Re numbers. Through the analysis of the normalised mean horizontal velocity, $\bar{u}_n(x, y)$, in five points of the plane, three error indexes have been introduced: FP, IRE and ISE, whose definition is described below

$$FP = min(i) \; \Bigg| \; |e(i,j)| = \left|\frac{\bar{u}_n^{i,j} - \bar{u}_n^{N_{max}}}{\bar{u}_n^{N_{max}}}\right| < 5\% \quad \forall j \in 1,2,...,5 \;\; and \;\; for \; i = 1,2,\ldots,N_{max} \tag{5}$$

$$IRE = \sum_{j=1}^{5} \sum_{i=1}^{N_{max}} \left|\frac{\bar{u}_n^{i,j} - \bar{u}_n^{N_{max}}}{\bar{u}_n^{N_{max}}}\right| \tag{6}$$

$$ISE = \sum_{j=1}^{5} \sum_{i=1}^{N_{max}} \left(\frac{\bar{u}_n^{i,j} - \bar{u}_n^{N_{max}}}{\bar{u}_n^{N_{max}}}\right)^2 \tag{7}$$

N_{max} represents the maximum number of image pairs used for the flow reconstruction. In this work, it has been set to 500 and it has been considered as correct; i.e. the mentioned value represents the velocity employed to evaluate the error (e(i,j)). Hence, the FP index indicates the minimum number of frame pairs "i" required by the diagnostic technique to achieve an error lower than the 5%, in each point analysed, whereas the IRE and ISE indexes are the sum of the relative and square errors, respectively, committed in all the five points and for all the frame pairs. These indexes have been evaluated for the GPV and µPIV tests, carried out on both the devices and for all the fluid-dynamic states (see Sec. 0). The results have been summarised in Figure 9, where each index is plotted as a function of the Reynolds number, for both the devices' size. The indexes are calculated in five points spread on the investigated plane (see Sec.0), and the legend displayed in the FP index's plot (Figure 9A) is valid for all the diagrams.

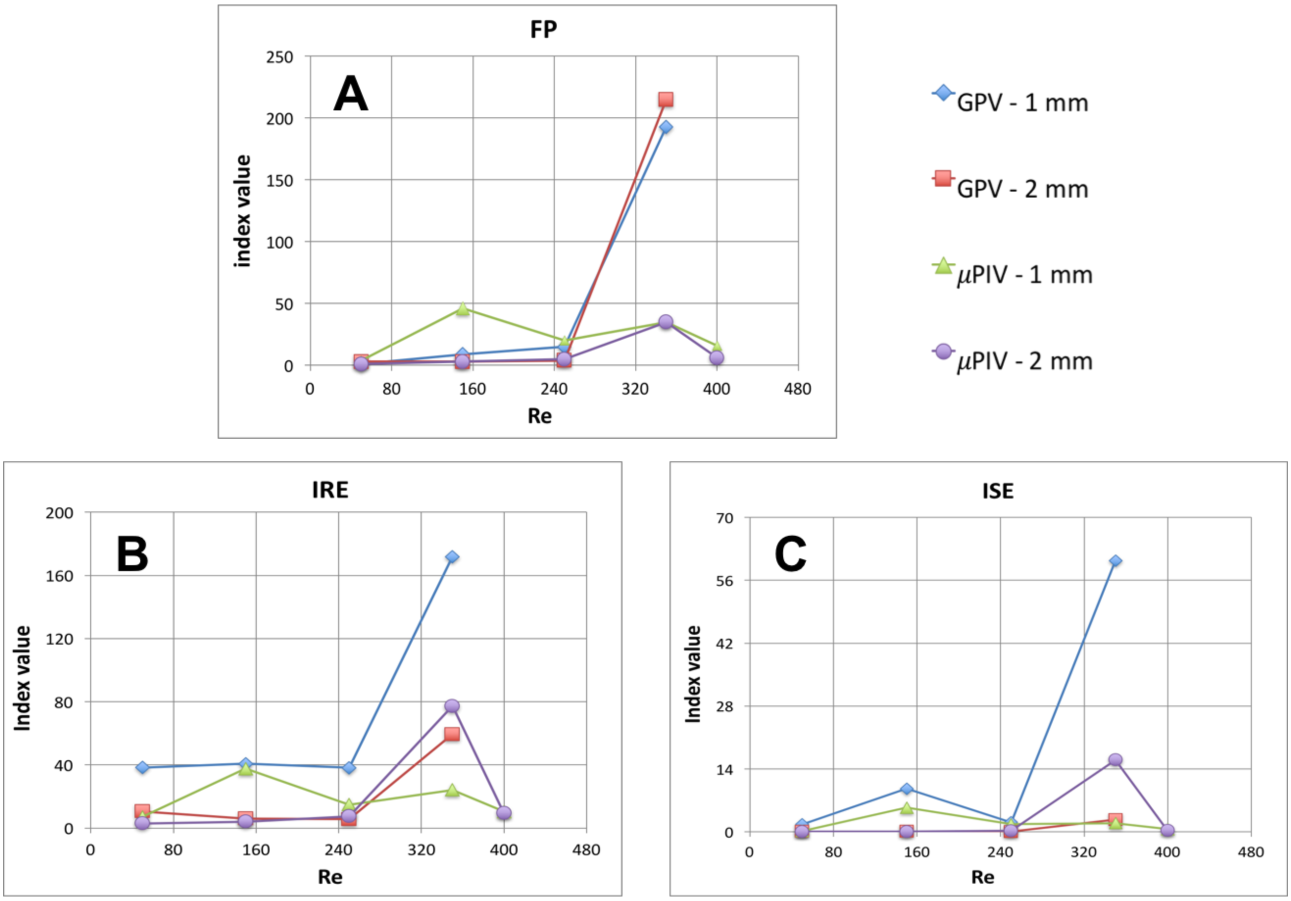

Figure 9: Trend of the error performance indexes defined from steady state and stability validation.

There are several indications that could be extracted from the charts:

(i) The performance of the GPV is strongly dependent on the Reynolds number, all the error indexes rapidly increase when the Re = 350. Instead, the µPIV is basically independent on the fluid-dynamic regime;

(ii) At Re=400 the GPV cannot achieve a proper result, the values of the velocity fluctuate too much and were unstable. The µPIV is able to produce a reliable result also at this inlet volumetric flow rate;

(iii) The µPIV shows comparable results for both device sizes, while the GPV has better results for the 2 mm one as the flow velocity is lower;

(iv) At low Reynolds numbers the two optical techniques have the same performance, considering that the indexes practically assume the same values.

All these considerations bring us to conclude that the performance of GPV deteriorates at higher Re numbers, while µPIV is efficient in all the explored cases. The reason can be immediately understood thinking about the different technologies of the cameras. The GPV utilises a high-speed camera which records a "continuous" frame sequence, where the frames are spaced out in time by the (inverse of) camera's frame rate (see Sec. 0). When the fluid flow speed is increased, a higher frame rate has to be used for the experiments as the recorded images have a lower quality. Furthermore, the electronic noise also diminishes the speckle pattern’s intensity which leads to poor performance in delivering results. This phenomenon does not occur in µPIV, where the synchronisation system precisely releases the camera's frame rate to the set Δt.

Conclusions

GPV is a novel technique, recently developed (Buzzaccaro et al., 2013) and implemented in a very few number of fluid-dynamic investigations (Kovalchuk et al., 2018; Martino et al., 2016; Pirbodaghi et al., 2015). Thus its capability in the visualisation of a complex flow velocity field needs further assessment. This work focused on optimising the experimental setup to test the capabilities of GPV starting from the peculiar device preparation, the optimal microscope setup, the frame rate selection, etc.., and the final results could be considered extremely satisfying. The flow velocity fields studied were compared and validated with results obtained using µPIV for Reynolds numbers ranging from 50 to 400 and for two characteristic sizes of the channel. Furthermore, the steady state regime validation and the outcomes convergence, which have also permitted to compare the performance between the velocimetry techniques, have demonstrated the consistency of the results. All the tests carried out allowed deducing some interesting conclusions:

(i) At low Reynolds numbers the GPV shows comparable results with the µPIV, in terms of flow mapping and performance;

(ii) The GPV performance is strongly influenced by the camera's performance. With the current fast camera setup for example, increasing the frame rate reduces the resolution and the electronic noise increases, reducing the contrast of the speckle pattern, thus the images become very noisy and the reconstruction is harder. This makes the technique less suitable for fast fluid flow phenomena, whereas the µPIV is only limited by the laser's pulse duration;

(iii) Decreasing the device's scale the GPV becomes more competitive, since the speckle pattern is easier to "recognise" as the speckles size is essentially independent on the optical magnification. When the size of the channel is reduced a higher objective magnification has to be used, therefore the speckles look bigger on the camera's field of view and are simpler to detect. The implementation of the µPIV is, instead, more complicated in very small devices, considering that the particle's size has to drop to hundreds of nanometres, where a high-power laser is required for the analysis.

Various features should be improved in the GPV implementation, first of all the cross-correlation (Adrian and Westerweel, 2007) and images processing algorithms. The PIVlab tool is a MATLAB routine designed for the dark images attained by the PIV analysis. A dedicated script, expressly designed for the GPV's bright field frames, might be elaborated to optimise the image processing. It would be extremely useful to create a unique software, where the complete reconstruction procedure may be managed, starting from the sequence acquisition until the velocity field visualisation. This would strongly decrease, together with the optimised image processing algorithm, the post processing time which is currently longer than the time required for the µPIV analyses. As previously described, the major limit for the technique is the high camera's frame rate required to characterise fast processes. The application of a synchroniser unit to the experimental setup would permit to overtake this obstacle. However, all the experiments and validations carried out permit us to affirm that the GPV has the potential to become, if further developed, a reliable and economical 3D flow visualisation technique for micro/milli-fluidic sized applications, in several scientific disciplines. An excellent alternative to the µPIV, which can turn into an economical and reliable research tool, especially in the classical low Reynolds regime, typically encountered for instance in microfluidic devices for medical and bioscience applications.

Acknowledgements

DV acknowledges the Royal Society Research Grant 2017 R1 (RG160698) for partially funding this research.

Bibliography

Adrian, R.J., Westerweel, J., 2007. Particle Image Velocimetry, Experimental Fluid Mechanics. Springer Berlin Heidelberg, Berlin, Heidelberg. doi:10.1007/978-3-540-72308-0

Asakura, T., Takai, N., 1981. Dynamic Laser Speckles and Their Application to Velocity Measurements of the Diffuse Object. Appl. Phys 25, 179–194.

Ault, J.T., Fani, A., Chen, K.K., Shin, S., Gallaire, F., Stone, H.A., 2016. Vortex-Breakdown-Induced Particle Capture in Branching Junctions. Phys. Rev. Lett. 117, 84501. doi:10.1103/PhysRevLett.117.084501

Benjamin, B.T.B., Benjamin, T.B., 1962. Theory of the vortex breakdown phenomenon.

Bothe, D., Lojewski, A., Warnecke, H.-J., 2011. Fully resolved numerical simulation of reactive mixing in a T-shaped micromixer using parabolized species equations. Chem. Eng. Sci. 66, 6424–6440. doi:10.1016/j.ces.2011.08.045

Bothe, D., Stemich, C., Warnecke, H.-J., 2006. Fluid mixing in a T-shaped micro-mixer. Chem. Eng. Sci. 61, 2950–2958. doi:10.1016/j.ces.2005.10.060

Brossard, C., Monnier, J.-C., Barricau, P., Vandernoot, F.-X., Sant, Y. Le, Champagnat, F., Besnerais, G. Le, 2009. Principles and applications of particle image velocimetry. Onera AerospaceLab J. AL01-03, 1–11.

Buzzaccaro, S., Secchi, E., Piazza, R., 2013. Ghost Particle Velocimetry: Accurate 3D Flow Visualization Using Standard Lab Equipment. Phys. Rev. Lett. 111, 48101. doi:10.1103/PhysRevLett.111.048101

Cederquist, J.N., Fienup, J.R., Marron, J.C., Paxman, R.G., 1988. Phase retrieval from experimental far-field speckle data. Opt. Lett. 13.

Chen, K.K., Rowley, C.W., Stone, H.A., 2015. Vortex dynamics in a pipe T-junction: Recirculation and sensitivity. Phys. Fluids 27, 34107. doi:10.1063/1.4916343

Dainty, J.C., 1975. Laser speckle and related phenomena. Springer-Verlag.

Engler, M., Kockmann, N., Kiefer, T., Woias, P., 2004. Numerical and experimental investigations on liquid mixing in static micromixers. Chem. Eng. J. 101, 315–322. doi:10.1016/J.CEJ.2003.10.017

Fani, A., Camarri, S., Salvetti, M.V., 2014. Unsteady asymmetric engulfment regime in a T-mixer. Phys.

Fluids 26, 74101. doi:10.1063/1.4885451

Fani, A., Camarri, S., Salvetti, M.V., 2013. Investigation of the steady engulfment regime in a three-dimensional T-mixer. Phys. Fluids 25, 64102. doi:10.1063/1.4809591

Galletti, C., Arcolini, G., Brunazzi, E., Mauri, R., 2015. Mixing of binary fluids with composition-dependent viscosity in a T-shaped micro-device. Chem. Eng. Sci. 123, 300–310. doi:10.1016/j.ces.2014.11.025

Galletti, C., Brunazzi, E., Mauri, R., 2017. Unsteady mixing of binary liquid mixtures with composition-dependent viscosity. Chem. Eng. Sci. 164, 333–343. doi:10.1016/j.ces.2017.02.035

Galletti, C., Roudgar, M., Brunazzi, E., Mauri, R., 2012. Effect of inlet conditions on the engulfment pattern in a T-shaped micro-mixer. Chem. Eng. J. 185–186, 300–313. doi:10.1016/j.cej.2012.01.046

Hall, M.G., 1972. Vortex Breakdown. Annu. Rev. Fluid Mech. 4, 195–218. doi:10.1146/annurev.fl.04.010172.001211

Hessel, V., Löwe, H., Schönfeld, F., 2005. Micromixers—a review on passive and active mixing principles. Chem. Eng. Sci. 60, 2479–2501. doi:10.1016/j.ces.2004.11.033

Hoffmann, M., Schlüter, M., Räbiger, N., 2006. Experimental investigation of liquid-liquid mixing in T-shaped micro-mixers using µ-LIF and µ-PIV. Chem. Eng. Sci. 61, 2968–2976. doi:10.1016/j.ces.2005.11.029

Jahanmiri, M., 2011. Particle Image Velocimetry: Fundamentals and Its Applications. Göteborg, Sweden.

Kockmann, N., Kiefer, T., Engler, M., Woias, P., 2006. Convective mixing and chemical reactions in microchannels with high flow rates. Sensors Actuators B Chem. 117, 495–508. doi:10.1016/J.SNB.2006.01.004

Kovalchuk, N.M., Chowdhury, J., Schofield, Z., Vigolo, D., Simmons, M.J.H., 2018. Study of drop coalescence and mixing in microchannel using Ghost Particle Velocimetry. Chem. Eng. Res. Des. doi:10.1016/j.cherd.2018.01.034

Lee, C.-Y., Wang, W.-T., Liu, C.-C., Fu, L.-M., 2016. Passive mixers in microfluidic systems: A review. Chem. Eng. J. 288, 146–160. doi:10.1016/j.cej.2015.10.122

Lindken, R., Westerweel, J., Wieneke, B., 2006. Stereoscopic micro particle image velocimetry. Exp. Fluids 41, 161–171. doi:10.1007/s00348-006-0154-5

Mariotti, A., Galletti, C., Mauri, R., Salvetti, M.V., Brunazzi, E., 2018. Steady and unsteady regimes in a T-shaped micro-mixer: synergic experimental and numerical investigation. Chem. Eng. J. doi:10.1016/j.cej.2018.01.108

Martino, C., Vigolo, D., Solvas, X.C. i, Stavrakis, S., DeMello, A.J., 2016. Real-Time PEGDA-Based Microgel Generation and Encapsulation in Microdroplets. Adv. Mater. Technol. 1, 1600028.

doi:10.1002/admt.201600028

Orsi, G., Galletti, C., Brunazzi, E., Mauri, R., 2013a. Mixing of two miscible liquids in T-shaped microdevices. Chem. Eng. Trans. 32, 1471–1476. doi:10.33032/CET1332246

Orsi, G., Roudgar, M., Brunazzi, E., Galletti, C., Mauri, R., 2013b. Water-ethanol mixing in T-shaped microdevices. Chem. Eng. Sci., 1 95, 174–183. doi:10.1016/j.ces.2013.03.015

Pirbodaghi, T., Vigolo, D., Akbari, S., DeMello, A., 2015. Investigating the fluid dynamics of rapid processes within microfluidic devices using bright-field microscopy. Lab Chip 15, 2140–2144. doi:10.1039/C5LC00175G

Poole, R.J., Alfateh, M., Gauntlett, A.P., 2013. Bifurcation in a T-channel junction: Effects of aspect ratio and shear-thinning. Chem. Eng. Sci. 104, 839–848. doi:10.1016/j.ces.2013.10.006

Roberge, D.M., Ducry, L., Bieler, N., Cretton, P., Zimmermann, B., 2005. Microreactor Technology: A Revolution for the Fine Chemical and Pharmaceutical Industries? Chem. Eng. Technol. 28, 318–323. doi:10.1002/ceat.200407128

Rossetti, I., Compagnoni, M., 2016. Chemical reaction engineering, process design and scale-up issues at the frontier of synthesis: Flow chemistry. Chem. Eng. J. 296, 56–70. doi:10.1016/j.cej.2016.02.119

Soleymani, A., Kolehmainen, E., Turunen, I., 2008. Numerical and experimental investigations of liquid mixing in T-type micromixers. Chem. Eng. J. 135, 219–228. doi:10.1016/j.cej.2007.07.048

Thielicke, W., Stamhuis, E.J., 2014. PIVlab – Towards User-friendly, Affordable and Accurate Digital Particle Image Velocimetry in MATLAB. J. Open Res. Softw. 2. doi:10.5334/jors.bl

Thomas, S., Ameel, T.A., 2010. An experimental investigation of moderate reynolds number flow in a T-Channel. Exp. Fluids 49, 1231–1245. doi:10.1007/s00348-010-0863-7

Vigolo, D., Griffiths, I.M., Radl, S., Stone, H.A., 2013. An experimental and theoretical investigation of particle--wall impacts in a T-junction. J. Fluid Mech. 727, 236–255. doi:10.1017/jfm.2013.200

Vigolo, D., Radl, S., Stone, H.A., 2014. Unexpected trapping of particles at a T junction. Proc. Natl. Acad. Sci. U. S. A. 111, 4770–4775. doi:10.1073/pnas.1321585111